

Coherence length in a dilute flat-band superconductor

M. Iskin

Department of Physics, Koç University, Rumelifeneri Yolu, 34450 Sarıyer, İstanbul, Türkiye

(Dated: July 12, 2024)

To explore the influence of quantum-geometric effects on the Ginzburg-Landau coherence length in a dilute flat-band superconductor, we adopt a BCS-BEC crossover approach to the multiband pyrochlore-Hubbard model near the critical temperature for superconductivity. Our self-consistent formulation for this three-dimensional lattice benchmarks very well against the so-called zero-temperature coherence length, demonstrating the monotonic decay of the coherence length to zero as the interaction strength increases. Additionally, we show that the effective mass of the many-body bound states (i.e., Cooper pairs) is nearly identical to that of the lowest-lying two-body bound states in the dilute flat-band limit.

I. INTRODUCTION

Recent theoretical studies have uncovered a surprising link between the quantum geometry of Bloch states and superconductivity in multiband systems, significantly advancing our understanding of the Cooper-pairing mechanism in flat-band systems [1, 2]. Under certain restrictive conditions, such as time-reversal symmetry and uniform pairing, it has been revealed that the quantum-metric tensor plays a critical role in determining key observables. These include the superfluid weight, superfluid density, critical transition temperature, low-energy collective Goldstone and Leggett modes, Ginzburg-Landau (GL) coherence length, London penetration depth, GL parameter, and upper critical magnetic field [1–11]. The common factor among these observables is the effective mass of the superfluid carriers [12, 13]. Despite the infinite band mass of particles in the underlying flat band, even an infinitesimal interaction gives Cooper pairs a finite effective mass through virtual interband transitions mediated by the quantum metric. This mechanism facilitates the emergence of superconductivity in a flat band in the presence of other bands [14]. Furthermore, the geometric origin is most evident in the effective mass of the lowest-lying two-body bound states, as demonstrated by exact calculations [15].

In multiband superconductors, geometric effects, while inherent, are generally overshadowed by conventional effects in the BCS limit [1, 2]. However, as the bandwidth of a Bloch band narrows, conventional effects diminish due to their dependence on the derivative of the Bloch bands. In contrast, geometric effects, which are determined by the derivative of the Bloch states, can become dominant under these conditions. Inspired by recent technological advances in creating two-dimensional materials with nearly-flat electronic bands [16], there is a growing surge of interest in understanding geometric effects in multiband superconductors [17–19]. Among them, there has been a perplexing GL study regarding the size of Cooper pairs in a flat-band superconductor, suggesting they are limited by a fundamental length scale determined by the quantum geometry of the flat band [20]. However, subsequent work using the Bogoliubov-de Gennes approach for various lattice mod-

els in one and two dimensions has demonstrated that characteristic correlation lengths can be smaller than one lattice spacing without being constrained by the quantum metric [21].

To address these discrepancies [20, 21], we investigate the quantum-geometric effects on the GL coherence length in a dilute flat-band superconductor using a BCS-BEC crossover approach to the multiband pyrochlore-Hubbard model near the critical temperature for pairing. Our self-consistent results are in good agreement with the zero-temperature coherence length, demonstrating that GL coherence length decreases to zero monotonously as the interaction strength increases. In addition, we find that the effective mass of Cooper pairs aligns closely with that of the lowest-lying two-body bound states in the dilute regime. The pyrochlore lattice, akin to well-studied two-dimensional models like the Mielke-checkerboard and kagome lattices known for uniform pairing, provides an ideal framework for exploring three-dimensional flat-band superconductivity [6]. Recent demonstrations of flat bands and superconductivity in materials like pyrochlore metal CaNi_2 [18] and pyrochlore superconductor CeRu_2 [19] underscore the relevance of this model.

The rest of the paper is organized as follows. In Sec. II, we introduce the multiband Hubbard Hamiltonian in reciprocal space, review the effective-action formalism near T_c , and derive the expansion coefficients for the time-dependent-GL (TDGL) theory. In Sec. III, we discuss self-consistency relations that are used to study dilute flat-band superconductivity in the pyrochlore lattice. In Sec. IV, we introduce the zero-temperature coherence length. In Sec. V, we present the numerical results and analyze them in various limits. The paper ends with a summary and outlook in Sec. VI, and the breakdown of zero-temperature coherence length is discussed in the Appendix.

II. TDGL THEORY

Having the pyrochlore-Hubbard model that we recently studied at zero temperature ($T = 0$) in mind [6], we begin by introducing the multiband Hubbard model

with an onsite attractive interaction and generic hopping terms. We then review the derivation of the effective action near the critical temperature T_c for superconductivity and apply the resultant TDGL theory to the pyrochlore lattice, which exhibits time-reversal symmetry and uniform pairing.

A. Multiband Hubbard Hamiltonian

Just as the kagome lattice is a line graph of the honeycomb lattice and the Mielke checkerboard lattice is a line graph of the square lattice, both of which feature a flat tight-binding band in two dimensions, the pyrochlore lattice is a line graph of the diamond lattice and it features two degenerate flat bands in three dimensions. Its crystal structure consists of a face-centered-cubic Bravais lattice with a four-point basis, leading to a truncated-octahedron shaped Brillouin Zone (BZ) [6]. This is in such a way that the total number of lattice sites is $N = 4N_c$, where $N_c = \sum_{\mathbf{k} \in \text{BZ}} 1$ counts the number of unit cells in real space, with $\mathbf{k} = (k_x, k_y, k_z)$ denoting the crystal momentum in units of $\hbar \rightarrow 1$.

Upon Fourier transformation from the site representation to the reciprocal space, the multiband Hubbard model becomes

$$\mathcal{H} = \sum_{SS'\mathbf{k}\sigma} \psi_{S\mathbf{k}\sigma}^\dagger (h_{SS'}^{\mathbf{k}\sigma} - \mu_\sigma \delta_{SS'}) \psi_{S'\mathbf{k}\sigma} - \frac{U}{N_c} \sum_{S\mathbf{k}\mathbf{k}'\mathbf{q}} \psi_{S\mathbf{k}\uparrow}^\dagger \psi_{S,-\mathbf{k}+\mathbf{q},\downarrow}^\dagger \psi_{S,-\mathbf{k}'+\mathbf{q},\downarrow} \psi_{S\mathbf{k}'\uparrow}, \quad (1)$$

where $\psi_{S\mathbf{k}\sigma}^\dagger$ creates a spin $\sigma = \{\uparrow, \downarrow\}$ particle on the sublattice $S = \{A, B, C, D\}$ and δ_{ij} is a Kronecker delta. Here, $U \geq 0$ is the strength of the attractive onsite interaction between \uparrow and \downarrow particles, and μ_σ is the chemical potential determining their average numbers in the ensemble. In the specific case of the pyrochlore lattice, which is our primary interest in this paper, the matrix elements of the Bloch Hamiltonian $\mathbf{h}_{\mathbf{k}\sigma}$ can be written as $h_{SS}^{\mathbf{k}\sigma} = 0$, $h_{AB}^{\mathbf{k}\sigma} = -2\bar{t} \cos\left(\frac{k_y+k_z}{4}a\right)$, $h_{AC}^{\mathbf{k}\sigma} = -2\bar{t} \cos\left(\frac{k_x+k_z}{4}a\right)$, $h_{AD}^{\mathbf{k}\sigma} = -2\bar{t} \cos\left(\frac{k_x+k_y}{4}a\right)$, $h_{BC}^{\mathbf{k}\sigma} = -2\bar{t} \cos\left(\frac{k_x-k_y}{4}a\right)$, $h_{BD}^{\mathbf{k}\sigma} = -2\bar{t} \cos\left(\frac{k_x-k_z}{4}a\right)$ and $h_{CD}^{\mathbf{k}\sigma} = -2\bar{t} \cos\left(\frac{k_y-k_z}{4}a\right)$, where \bar{t} is the tight-binding hopping parameter between the nearest-neighbor sites and a is the side-length of the conventional simple-cubic cell [6]. Thus, the Bloch bands are determined by $\sum_{S'} h_{SS'}^{\mathbf{k}\sigma} n_{S'\mathbf{k}\sigma} = \varepsilon_{n\mathbf{k}\sigma} n_{S\mathbf{k}\sigma}$, leading to $\varepsilon_{1\mathbf{k}\sigma} = -2\bar{t}(1 + \sqrt{1 + \alpha_{\mathbf{k}}})$ and $\varepsilon_{2\mathbf{k}\sigma} = -2\bar{t}(1 - \sqrt{1 + \alpha_{\mathbf{k}}})$ for the dispersive bands, where $\alpha_{\mathbf{k}} = \cos(k_x a/2) \cos(k_y a/2) + \cos(k_y a/2) \cos(k_z a/2) + \cos(k_x a/2) \cos(k_z a/2)$, and $\varepsilon_{3\mathbf{k}\sigma} = \varepsilon_{4\mathbf{k}\sigma} = 2\bar{t}$ for the degenerate flat bands. Note that $\varepsilon_{2\mathbf{k}\sigma}$ touches the flat bands at $\mathbf{k} = \mathbf{0}$. To ensure that these flat bands appear at the bottom of the Bloch spectrum, we set $\bar{t} \rightarrow -\bar{t}$ and choose $t > 0$ as the unit of energy. This allows us to construct a relatively simple BCS-BEC crossover formalism for a dilute flat-band superconductor near T_c , and study some of

its properties as functions of U . Here, $n_{S\mathbf{k}\sigma} = \langle S | n_{\mathbf{k}\sigma} \rangle$ is the sublattice projection of the Bloch state $|n_{\mathbf{k}\sigma}\rangle$, which plays an important role throughout this paper.

B. Effective action near $T \leq T_c$

In order to construct a microscopic TDGL theory near T_c [22], we first extract the effective free-energy density of the system per lattice site as a function of the pairing order parameter from the effective action, i.e., from $\frac{T}{N}(S_2 + S_4)$, where T is the temperature in units of the Boltzmann constant $k_B \rightarrow 1$, and S_2 (S_4) is the quadratic (quartic) contribution to the action [5]. The saddle-point action S_0 is not needed here because it does not depend on the order parameter at T_c , and S_1 and S_3 vanish at any T due to the saddle-point condition.

Using the Grassmann functional-integral formalism, one can show that $\mathcal{S}_2 = \frac{N_c}{T} \sum_{SS'q} \Lambda_S^*(q) \Gamma_{SS'}^{-1}(q) \Lambda_{S'}(q)$ [5], where $q \equiv (\mathbf{q}, i\nu_\ell)$ is a collective index with $\nu_\ell = 2\ell\pi T$ denoting the bosonic Matsubara frequency, $\Lambda_S(q)$ plays the role of the pairing order parameter for sublattice S , and

$$\Gamma_{SS'}^{-1}(q) = \frac{\delta_{SS'}}{U} + \frac{1}{2N_c} \sum_{nm\mathbf{k}} \frac{\mathcal{X}_{n\mathbf{k}\uparrow} + \mathcal{X}_{m,-\mathbf{k}+\mathbf{q},\downarrow}}{i\nu_\ell - \xi_{n\mathbf{k}\uparrow} - \xi_{m,-\mathbf{k}+\mathbf{q},\downarrow}} \times n_{S\mathbf{k}\uparrow} n_{S'\mathbf{k}\uparrow}^* m_{S',-\mathbf{k}+\mathbf{q},\downarrow}^* m_{S,-\mathbf{k}+\mathbf{q},\downarrow}, \quad (2)$$

is the matrix element of the inverse pair-fluctuation propagator $\Gamma^{-1}(q)$. Here, $\mathcal{X}_{n\mathbf{k}\sigma} = \tanh\left(\frac{\xi_{n\mathbf{k}\sigma}}{2T}\right)$ is a thermal factor and $\xi_{n\mathbf{k}\sigma} = \varepsilon_{n\mathbf{k}\sigma} - \mu_\sigma$. This propagator suggests that the generalized Thouless condition $\det \Gamma^{-1}(\mathbf{q}, 0) = 0$ determines T_c of a multiband Hubbard model for any center-of-mass momentum \mathbf{q} . For instance, $T_c = \max\{T_{c1}, T_{c2}, T_{c3}, T_{c4}\}$ in the case of the pyrochlore lattice, where T_{c_j} is determined by setting the j th eigenvalue of $\Gamma^{-1}(\mathbf{q}, 0)$ to 0. In our numerical calculations, we observed that $T_{c1} > T_{c2} = T_{c3} = T_{c4}$ for any given set of $(\mu_\uparrow = \mu_\downarrow, U)$ in the $\mathbf{q} \rightarrow \mathbf{0}$ limit. Furthermore, we observed that the associated eigenvector of $\Gamma^{-1}(\mathbf{q}, 0)$ that corresponds to the T_{c1} solution is uniform in a unit cell, i.e., $[\Lambda_A(\mathbf{q}), \Lambda_B(\mathbf{q}), \Lambda_C(\mathbf{q}), \Lambda_D(\mathbf{q})] = \Lambda_0(\mathbf{q})[1, 1, 1, 1]$ in the $\mathbf{q} \rightarrow \mathbf{0}$ limit. It is pleasing to note that the latter observation aligns perfectly with our previous finding that the uniform-pairing condition is satisfied exactly for the lowest-lying two-body bound states of the pyrochlore lattice when $\mathbf{q} \rightarrow \mathbf{0}$ [6].

Motivated by these numerical insights and to facilitate further analytical progress, we next adopt the following assumptions that are satisfied by the pyrochlore lattice. (i) The lattice manifests time-reversal symmetry, leading to $n_{S,-\mathbf{k},\downarrow}^* = n_{S\mathbf{k}\uparrow} = n_{S\mathbf{k}}$ and $\xi_{n,-\mathbf{k},\downarrow} = \xi_{n\mathbf{k}\uparrow} = \xi_{n\mathbf{k}}$. (ii) The low- q order parameters are uniform in a unit cell, leading to $\Lambda_0(q) = \Lambda_S(q)$ for all sublattices. Under these assumptions, the quadratic action can be written

as $\mathcal{S}_2 = \frac{N}{T} \sum_q \Gamma_0^{-1}(q) |\Lambda_0(q)|^2$ [5], where

$$\Gamma_0^{-1}(q) = \frac{1}{U} + \frac{1}{2N} \sum_{nm\mathbf{k}} \frac{\mathcal{X}_{n\mathbf{k}} + \mathcal{X}_{m,\mathbf{k}-\mathbf{q}}}{i\nu_\ell - \xi_{n\mathbf{k}} - \xi_{m,\mathbf{k}-\mathbf{q}}} |\langle n_{\mathbf{k}} | m_{\mathbf{k}-\mathbf{q}} \rangle|^2. \quad (3)$$

Thus, the Thouless condition reduces to $\Gamma_0^{-1}(\mathbf{0}, 0) = 0$ for stationary BCS-type pairing, determining T_c of a uniformly-paired multiband Hubbard model in the presence of time-reversal symmetry. Similarly, by making use of the Grassmann functional-integral formalism, and under the same assumptions discussed above, one can approximate that $\mathcal{S}_4 = \frac{Nb_0}{2T} \sum_{q_1 q_2 q_3} \Lambda_0^*(q_1 + q_2 + q_3) \Lambda_0(q_1) \Lambda_0^*(-q_2) \Lambda_0(q_3)$ [5]. Here, a positive b_0 coefficient not only guarantees the energetic stability of the TDGL theory, but it also characterizes the repulsive interaction between Cooper pairs as discussed next.

C. Coefficients for the TDGL expansion

When $T \lesssim T_c$, the coefficients for the microscopic TDGL theory can be determined through the expansion of the inverse propagator $\Gamma_0^{-1}(\mathbf{q}, i\nu_\ell \rightarrow \omega + i0^+) = -a_0\epsilon(T) + \frac{1}{2} \sum_{ij} c_{ij} q_i q_j + d\omega + \dots$ in the low- (\mathbf{q}, ω) regime, where $\epsilon(T) = (T_c - T)/T_c$ changes sign across T_c in accordance with the Landau theory of second-order phase transitions [5, 22]. This expansion leads to

$$a_0 = \frac{1}{N} \sum_{n\mathbf{k}} \left[\frac{\mathcal{Y}_{n\mathbf{k}}}{4T_c} + \frac{\partial \mu}{\partial T} \left(\frac{\mathcal{Y}_{n\mathbf{k}}}{4\xi_{n\mathbf{k}}} - \frac{T_c \mathcal{X}_{n\mathbf{k}}}{2\xi_{n\mathbf{k}}^2} \right) \right], \quad (4)$$

$$b_0 = \frac{1}{N} \sum_{n\mathbf{k}} \left(\frac{\mathcal{X}_{n\mathbf{k}}}{4\xi_{n\mathbf{k}}^3} - \frac{\mathcal{Y}_{n\mathbf{k}}}{8T_c \xi_{n\mathbf{k}}^2} \right), \quad (5)$$

$$c_{ij}^{\text{intra}} = \frac{1}{N} \sum_{n\mathbf{k}} \left(\frac{\mathcal{X}_{n\mathbf{k}}}{4\xi_{n\mathbf{k}}^3} - \frac{\mathcal{Y}_{n\mathbf{k}}}{8T_c \xi_{n\mathbf{k}}^2} \right) \xi_{n\mathbf{k}}^i \xi_{n\mathbf{k}}^j, \quad (6)$$

$$c_{ij}^{\text{inter}} = \frac{1}{N} \sum_{n\mathbf{k}} \frac{\mathcal{X}_{n\mathbf{k}}}{2\xi_{n\mathbf{k}}} g_{ij}^{n\mathbf{k}} - \frac{1}{2N} \sum_{n,m \neq n, \mathbf{k}} \frac{\mathcal{X}_{n\mathbf{k}} + \mathcal{X}_{m\mathbf{k}}}{\xi_{n\mathbf{k}} + \xi_{m\mathbf{k}}} g_{ij}^{nm\mathbf{k}}, \quad (7)$$

$$d = \frac{1}{N} \sum_{n\mathbf{k}} \frac{\mathcal{X}_{n\mathbf{k}}}{4\xi_{n\mathbf{k}}^2} + \frac{i\pi}{8T_c N} \sum_n D_n(\mu) \theta_\mu, \quad (8)$$

where $\mathcal{Y}_{n\mathbf{k}} = \text{sech}^2\left(\frac{\xi_{n\mathbf{k}}}{2T}\right)$ is a thermal factor and $\xi_{n\mathbf{k}}^i = \partial \xi_{n\mathbf{k}} / \partial k_i$. In order to reproduce the correct U_{pp} that is previously obtained from the low-energy collective-mode analysis at $T = 0$ [6], i.e., see Sec. V for further discussion, here the expansion coefficients are given per lattice site. We note that all of these coefficients must be evaluated at T_c self-consistently with μ . In addition, since the factor $\frac{\partial \mu}{\partial T}$ plays a crucial role away from the BCS limit, Eq. (4) has to be handled with care in flat-band superconductors, which is described in Sec. V. However, numerical implementation of the rest of the coefficients is a straightforward task once (μ, T_c) is computed for a desired U .

Motivated by the recent surge of interest in the quantum-geometric effects, here we also split the kinetic coefficient into two contributions $c_{ij} = c_{ij}^{\text{intra}} + c_{ij}^{\text{inter}}$, depending on whether the intraband or interband processes are involved. Note that, in comparison to our previous work [5], here we used integration by parts $\sum_{\mathbf{k}} \mathcal{X}_{n\mathbf{k}} \xi_{n\mathbf{k}}^{ij} / \xi_{n\mathbf{k}}^2 = \sum_{\mathbf{k}} [2\mathcal{X}_{n\mathbf{k}} / \xi_{n\mathbf{k}}^3 - \mathcal{Y}_{n\mathbf{k}} / (2T \xi_{n\mathbf{k}}^2)] \xi_{n\mathbf{k}}^i \xi_{n\mathbf{k}}^j$ and $\sum_{\mathbf{k}} \mathcal{Y}_{n\mathbf{k}} \xi_{n\mathbf{k}}^{ij} / \xi_{n\mathbf{k}} = \sum_{\mathbf{k}} [\mathcal{Y}_{n\mathbf{k}} / \xi_{n\mathbf{k}}^2 + \mathcal{X}_{n\mathbf{k}} \mathcal{Y}_{n\mathbf{k}} / (T \xi_{n\mathbf{k}})] \xi_{n\mathbf{k}}^i \xi_{n\mathbf{k}}^j$, and reexpressed c_{ij}^{intra} in the new form given by Eq. (6), where $\xi_{n\mathbf{k}}^{ij} = \partial^2 \xi_{n\mathbf{k}} / \partial k_i \partial k_j$. This coefficient is the so-called conventional contribution, as it is simply a sum over its single-band counterpart [5]. Similarly, the coefficients a_0 , b_0 and d are sums over their single-band counterparts. In contrast, the geometric contribution c_{ij}^{inter} is controlled by the quantum-metric tensor $g_{ij}^{n\mathbf{k}} = \sum_{n \neq m} g_{ij}^{nm\mathbf{k}}$ of the n th Bloch band [23–25] and its band-resolved quantum-metric tensor $g_{ij}^{nm\mathbf{k}} = 2\text{Re} \left[\langle \dot{n}_{\mathbf{k}}^i | m_{\mathbf{k}} \rangle \langle m_{\mathbf{k}} | \dot{n}_{\mathbf{k}}^j \rangle \right]$, where Re denotes the real part and $|\dot{n}_{\mathbf{k}}^i\rangle = \partial |n_{\mathbf{k}}\rangle / \partial k_i$. Such terms follow from the low- \mathbf{q} expansion of the Bloch factor

$$|\langle n_{\mathbf{k}} | m_{\mathbf{k}-\mathbf{q}} \rangle|^2 = \delta_{nm} - \frac{1}{2} \sum_{ij} [g_{ij}^{n\mathbf{k}} \delta_{nm} + g_{ij}^{nm\mathbf{k}} (\delta_{nm} - 1)] q_i q_j \quad (9)$$

that appears in Eq. (3). It is important to highlight that c_{ij}^{inter} does not have any contribution from the band touchings, i.e., the first term of Eq. (7) cancels those touching contributions from the second term whenever $\xi_{n\mathbf{k}} = \xi_{m\mathbf{k}}$ for any $n \neq m$. For instance, in the case of pyrochlore lattice, there is no inter-flat-band contribution to c_{ij}^{inter} among the degenerate flat bands as they touch each other everywhere in the BZ.

Furthermore, we note that the dynamic coefficient d is a complex number in general [5, 22], and its imaginary part is determined by the density of states $D_n(\varepsilon) = \sum_{\mathbf{k}} \delta(\varepsilon - \varepsilon_{n\mathbf{k}})$ of the n th Bloch band where $\theta_\varepsilon = \theta(\varepsilon - \min\{\varepsilon_{n\mathbf{k}}\})\theta(\max\{\varepsilon_{n\mathbf{k}}\} - \varepsilon)$. Here, $\delta(x)$ is the Dirac-delta distribution and $\theta(x)$ is the Heaviside-step function. Thus, d has a dominant positive imaginary part in the BCS limit when μ lies within any one of the Bloch bands. This is nothing but a reflection of the continuum of fermionic excitations into which a Cooper pair can decay, suggesting that the dynamics of the order parameter is overdamped in the BCS limit. In sharp contrast, d becomes purely real in the BEC limit suggesting that the dynamics of the order parameter is propagating. For the dilute flat-band superconductor of interest in this paper, the latter turns out to be the case for any $U \neq 0$.

Assuming this is the case, and by making an analogy with the Gross-Pitaevskii equation for a weakly-interacting atomic Bose gas, i.e., through a scaling of the order parameter [5, 22], we define $\mu_p(T) = a_0\epsilon(T)/d$ as the effective chemical potential of the Cooper pairs, $(M_p^{-1})_{ij} = c_{ij}/d$ as the inverse effective-mass tensor \mathbf{M}_p^{-1} of the pairs, and $U_{pp} = b_0/d^2$ as the effective on-

site repulsive interaction between the pairs. This identification suggests that \mathbf{M}_p is composed of a conventional contribution $(M_p^{-1})_{ij}^{\text{intra}} = c_{ij}^{\text{intra}}/d$ and a geometric one $(M_p^{-1})_{ij}^{\text{inter}} = c_{ij}^{\text{inter}}/d$. In this paper, we are primarily interested in the GL coherence length $(\xi_T^2)_{ij} = (\xi_{\text{GL}}^2)_{ij}/\epsilon(T)$, whose temperature-independent prefactor is given by

$$(\xi_{\text{GL}}^2)_{ij} = \frac{c_{ij}}{2a_0}. \quad (10)$$

This relation again suggests that ξ_{GL} is composed of a conventional contribution $(\xi_{\text{GL}}^2)_{ij}^{\text{intra}} = c_{ij}^{\text{intra}}/(2a_0)$ and a geometric one $(\xi_{\text{GL}}^2)_{ij}^{\text{inter}} = c_{ij}^{\text{inter}}/(2a_0)$. Since the calculation of ξ_{GL} requires μ and T_c as inputs, we next describe our recipe for their self-consistent evaluation as a function of U , which is appropriate for a dilute flat-band superconductor in the pyrochlore lattice.

III. SELF-CONSISTENCY RELATIONS: (μ, T_c)

As the simplest route, we follow the usual finite-temperature BCS-BEC crossover formalism [22, 26] to construct a self-consistent theory based on the Thouless condition, which is equivalent to both the saddle-point condition and the mean-field order-parameter equation, and the number equation $\mathcal{N} = -\partial\Omega/\partial\mu$. Here, Ω is the thermodynamic potential, and keeping its corrections at the Gaussian order, i.e., $\Omega_G = \Omega_0 + \Omega_2$, is known to be sufficient in producing a qualitatively correct physical description of the system for all $U \neq 0$.

One can show quite generally that $\Omega_0 = TS_0$ is the saddle-point and $\Omega_2 = T \sum_q \ln \det[T\mathbf{\Gamma}^{-1}(q)]$ is the quadratic contribution. At T_c , while the former leads to the Fermi-Dirac (FD) distribution of an unbound (free) Fermi gas of \uparrow and \downarrow fermions, the latter contribution is typically split into $\mathcal{N}_2 = \mathcal{N}_{bs} + \mathcal{N}_{sc}$ [22, 26]. While the bound-state contribution \mathcal{N}_{bs} arises from the isolated poles of $\mathbf{\Gamma}(q)$, the continuum of two-particle excitations leads to the scattering contribution \mathcal{N}_{sc} arising from the branch cut of the logarithm. Thus, $\mathcal{N}_{bs} = -T \sum_q \frac{\partial[\det \mathbf{\Gamma}^{-1}(q)]/\partial\mu}{\det \mathbf{\Gamma}^{-1}(q)}$ can be simplified considerably by noting that $\det \mathbf{\Gamma}^{-1}(q) \propto \Pi_s(i\nu_\ell - \omega_{s\mathbf{q}})$, where $\omega_{s\mathbf{q}}$ are the poles of $\mathbf{\Gamma}(q)$ determined by $\det \mathbf{\Gamma}^{-1}(\mathbf{q}, \omega_{s\mathbf{q}}) = 0$. For instance, since $\partial\omega_{s\mathbf{q}}/\partial\mu = -2$ in the BEC limit, one can approximate $\mathcal{N}_{bs} = -T \sum_{\ell s\mathbf{q}} 2/(i\nu_\ell - \omega_{s\mathbf{q}}) = 2 \sum_{s\mathbf{q}} f_{\text{BE}}(\omega_{s\mathbf{q}})$, after summing over the Matsubara frequencies, where $f_{\text{BE}}(x) = 1/(e^{x/T} - 1) = [\coth(\frac{x}{2T}) - 1]/2$ is the Bose-Einstein (BE) distribution of a bound Bose gas of Cooper pairs. On the other hand, the branch-cut contribution is given by $\mathcal{N}_{sc} = \sum_{\mathbf{q}} \int_{-\infty}^{+\infty} \frac{d\omega}{\pi} f_{\text{BE}}(\omega) \frac{\partial\delta(\mathbf{q}, \omega)}{\partial\mu}$, where $\delta(\mathbf{q}, \omega) = -\text{Arg}[\det \mathbf{\Gamma}^{-1}(\mathbf{q}, \omega + i0^+)]$ is the argument of the the propagator [22, 26]. For instance, if we decompose $\det \mathbf{\Gamma}^{-1}(\mathbf{q}, \omega + i0^+) = R + iI$ into its real and imaginary parts then $\frac{\partial\delta(\mathbf{q}, \omega)}{\partial\mu} = (\dot{R}^\mu I - R \dot{I}^\mu)/(R^2 + I^2)$, where

$\dot{R}^\mu = \partial R/\partial\mu$ and $\dot{I}^\mu = \partial I/\partial\mu$. Since accurately computing \mathcal{N}_{sc} is quite challenging, even in the context of much simpler continuum problems [22, 26], we next focus only on a dilute flat-band superconductor where \mathcal{N}_{sc} is negligible for all $U \neq 0$, and can be omitted.

Thus, having a dilute flat-band superconductor in the pyrochlore lattice in mind, our self-consistency relations for μ and T_c can be summarized as

$$1 = \frac{U}{N} \sum_{n\mathbf{k}} \frac{\mathcal{X}_{n\mathbf{k}}}{2\xi_{n\mathbf{k}}}, \quad (11)$$

$$F = \frac{2}{N} \sum_{n\mathbf{k}} f_{\text{FD}}(\xi_{n\mathbf{k}}) + \frac{2}{N} \sum_{\mathbf{q}} f_{\text{BE}}(\omega_{b\mathbf{q}}), \quad (12)$$

where $0 \leq F = \mathcal{N}/N \leq 2$ is the average filling of particles per lattice site and $f_{\text{FD}}(x) = 1/(e^{x/T} + 1) = [1 - \tanh(\frac{x}{2T})]/2$ is the FD distribution. In Eq. (12), the prefactor of 2 in front of the FD distribution is due to spin degeneracy, while that of the BE distribution can be traced back to the presence of 2 particles in a two-body bound state. Since the flat bands appear at the bottom of the Bloch spectrum in the pyrochlore lattice, we emphasize that Eq. (12) is very accurate in the $F \ll 1$ limit for all $U \neq 0$, but it may still give qualitatively correct results up to the half-filling for the flat bands, i.e., up to $F \lesssim 0.5$. In addition, it is, by construction, accurate for other multiband lattices up to their half fillings, i.e., up to $F \lesssim 1$, in the $U/t \gg 1$ limit. In Eq. (12), it is sufficient to keep only one of the pole contributions, i.e., the one with the lowest energy, because poles with higher energies are expected to give negligible contributions due to the BE distribution. Note that, in the presence of time-reversal symmetry and uniform pairing, this is also equivalent to keeping the isolated pole of Eq. (3). Furthermore, in our numerical calculations, we implement the simplest approach and extract $\omega_{b\mathbf{q}}$ from the dispersion $E_{1\mathbf{q}}$ of the lowest-lying two-body bound-state branch as follows.

In general, all of the two-body bound states can be determined from the isolated poles of Eq. (2) exactly, i.e., by computing $\det \mathbf{\Gamma}^{-1}(\mathbf{q}, E_{s\mathbf{q}}) = 0$, after setting the thermal factors $\mathcal{X}_{n\mathbf{k}\sigma} \rightarrow 1$ and $\mu \rightarrow 0$ [5]. However, in the presence of time-reversal symmetry and uniform pairing, the lowest-lying branch can simply be determined from the isolated pole of Eq. (3), i.e., by computing $\Gamma_0^{-1}(\mathbf{q}, E_{1\mathbf{q}}) = 0$, after again setting the thermal factors $\mathcal{X}_{n\mathbf{k}} \rightarrow 1$ and $\mu \rightarrow 0$. It can be shown that the overall structure of the two-body bound-state branches $E_{s\mathbf{q}}$ resemble the underlying Bloch bands $\varepsilon_{n\mathbf{k}}$ but with the opposite sign of energy [6]. For instance, $E_{1\mathbf{q}}$ resembles to $-\varepsilon_{1\mathbf{k}}$ but with an effective pair hopping parameter t_b and some energy offset depending on U . To determine these effective parameters, we first expand $\varepsilon_{1\mathbf{k}} = -6\bar{t} + a^2\bar{t}|\mathbf{k}|^2/8$ in the low $\mathbf{k} \rightarrow \mathbf{0}$ limit, and identify the relation between the hopping parameter and the effective mass m_1 of the unpaired spin- σ particles as $\bar{t} = 4/(a^2 m_1)$. This suggests that $t_b = 4/(a^2 M_b)$ is the relation between the effective hopping parameter and effective mass M_b of the lowest-lying two-body bound

states.

In the low- \mathbf{q} limit, we also recall that $E_{1\mathbf{q}} = E_b + \frac{1}{2} \sum_{ij} (M_b^{-1})_{ij} q_i q_j$ [15], where the energy offset E_b is determined by $1 = \frac{U}{N} \sum_{n\mathbf{k}} 1/(2\varepsilon_{n\mathbf{k}} - E_b)$. Furthermore, very similar to that of the many-body bound states discussed in Sec. II C, the inverse effective-mass tensor $(M_b^{-1})_{ij} = (M_b^{-1})_{ij}^{\text{intra}} + (M_b^{-1})_{ij}^{\text{inter}}$ of the lowest-lying two-body bound states is composed of an analogous conventional contribution $(M_b^{-1})_{ij}^{\text{intra}} = \frac{1}{2D} \sum_{n\mathbf{k}} \tilde{\varepsilon}_{n\mathbf{k}}^{ij}/(2\varepsilon_{n\mathbf{k}} - E_b)^2$ and an analogous geometric one $(M_b^{-1})_{ij}^{\text{inter}} = \frac{1}{D} \sum_{n\mathbf{k}} g_{ij}^{n\mathbf{k}}/(2\varepsilon_{n\mathbf{k}} - E_b) - \frac{1}{D} \sum_{n,m \neq n,\mathbf{k}} g_{ij}^{n\mathbf{k}m}/(\varepsilon_{n\mathbf{k}} + \varepsilon_{m\mathbf{k}} - E_b)$. It is important to emphasize that these two-body expressions are exact for any $U \neq 0$ in the pyrochlore lattice [6], and $(M_b^{-1})_{ij} = \delta_{ij}/M_b$ is diagonal as a consequence of uniform pairing. Thus, E_b and M_b can be determined self-consistently through these analytical expressions as functions of U , where $D = \sum_{n\mathbf{k}} 1/(2\varepsilon_{n\mathbf{k}} - E_b)^2$. Once E_b and M_b are determined, we identify that

$$\omega_{b\mathbf{q}} = E_{1\mathbf{q}} - 2\mu = \varepsilon_{b\mathbf{q}} - \mu_b, \quad (13)$$

leading to $\varepsilon_{b\mathbf{q}} = 6t_b - 2t_b(1 + \sqrt{1 + \alpha_{\mathbf{q}}})$ as the effective dispersion, where $\alpha_{\mathbf{q}}$ is defined in Sec. II A, and $\mu_b = 2\mu - E_b \rightarrow 0^-$ as the effective chemical potential of pairs, such that $\varepsilon_{b\mathbf{q}} = |\mathbf{q}|^2/(2M_b)$ reproduces the two-body physics exactly for all $U \neq 0$ in the low $\mathbf{q} \rightarrow \mathbf{0}$ limit. In Sec. V, we benchmark this approximate yet relatively complicated finite-temperature recipe against a much simpler zero-temperature one for the pyrochlore lattice, demonstrating very good agreement between the two.

IV. COHERENCE LENGTH AT $T = 0$

To compare with the GL coherence length ξ_{GL} , here we derive the so-called zero-temperature coherence length ξ_0 [27], based on the effective Gaussian action for the order-parameter fluctuations [6]. Using the Grassmann functional-integral formalism, and under the same assumptions discussed above, one can show that $\mathcal{S}_2 = \frac{N}{2T} \sum_q (\Lambda_q^* \Lambda_{-q}) \mathcal{M}^q \begin{pmatrix} \Lambda_q \\ \Lambda_{-q}^* \end{pmatrix}$ is the quadratic action, where the matrix \mathcal{M}^q plays the role of an inverse propagator for the fluctuations. The explicit finite-temperature expressions for its matrix elements, $\mathcal{M}_{11}^q = \mathcal{M}_{22}^{-q}$ and $\mathcal{M}_{12}^q = \mathcal{M}_{21}^q$, can be found in our previous work [6]. The off-diagonal terms vanish as $T \rightarrow T_c$, and the diagonal ones give rise to $\Gamma_0^{-1}(q)$.

We define ξ_0 by setting $\nu_\ell = 0$ and expanding $\mathcal{M}_{11}^q + \mathcal{M}_{12}^q$ at $T = 0$ up to second order in \mathbf{q} , corresponding to the amplitude-amplitude matrix element of the fluctuation propagator in the long-wavelength limit [27]. This

leads to $\mathcal{M}_{11}^q + \mathcal{M}_{12}^q = A + \sum_{ij} C_{ij} q_i q_j$ [6], where

$$A = \frac{1}{N} \sum_{n\mathbf{k}} \frac{\Delta_0^2}{2E_{n\mathbf{k}}^3}, \quad (14)$$

$$C_{ij}^{\text{intra}} = \frac{1}{N} \sum_{n\mathbf{k}} \frac{1}{8E_{n\mathbf{k}}^3} \left(1 - \frac{5\Delta_0^2 \xi_{n\mathbf{k}}^2}{E_{n\mathbf{k}}^4} \right) \dot{\xi}_{n\mathbf{k}}^i \dot{\xi}_{n\mathbf{k}}^j, \quad (15)$$

$$C_{ij}^{\text{inter}} = \frac{1}{N} \sum_{n\mathbf{k}} \frac{\xi_{n\mathbf{k}}^2}{4E_{n\mathbf{k}}^3} g_{ij}^{n\mathbf{k}} - \frac{1}{N} \sum_{n,m \neq n,\mathbf{k}} \frac{\xi_{n\mathbf{k}} \xi_{m\mathbf{k}} + E_{n\mathbf{k}} E_{m\mathbf{k}} - \Delta_0^2}{4E_{n\mathbf{k}} E_{m\mathbf{k}} (E_{n\mathbf{k}} + E_{m\mathbf{k}})} g_{ij}^{n\mathbf{k}m}, \quad (16)$$

Here, Δ_0 is the saddle-point, i.e., the mean-field, order parameter for pairing, and $E_{n\mathbf{k}} = \sqrt{\Delta_0^2 + \xi_{n\mathbf{k}}^2}$ is the quasi-particle energy associated with the n th Bloch band. In order to make a direct comparison with a_0 and c_{ij} discussed in Sec. II C, these expansion coefficients are also given per lattice site. Furthermore, we again split the kinetic coefficient into two contributions $C_{ij} = C_{ij}^{\text{intra}} + C_{ij}^{\text{inter}}$, depending on whether the intraband or interband processes are involved. This is in such a that the coefficients A and C_{ij}^{intra} are again simply sums over their conventional single-band counterparts [6, 27, 28]. The latter can be verified through the integration by parts $\sum_{\mathbf{k}} \xi_{n\mathbf{k}} \dot{\xi}_{n\mathbf{k}}^{ij}/E_{n\mathbf{k}}^3 = \sum_{\mathbf{k}} (3\xi_{n\mathbf{k}}^2 - E_{n\mathbf{k}}^2) \dot{\xi}_{n\mathbf{k}}^i \dot{\xi}_{n\mathbf{k}}^j / E_{n\mathbf{k}}^5$ and $\sum_{\mathbf{k}} \xi_{n\mathbf{k}} \dot{\xi}_{n\mathbf{k}}^{ij}/E_{n\mathbf{k}}^5 = \sum_{\mathbf{k}} (5\xi_{n\mathbf{k}}^2 - E_{n\mathbf{k}}^2) \dot{\xi}_{n\mathbf{k}}^i \dot{\xi}_{n\mathbf{k}}^j / E_{n\mathbf{k}}^7$ in Eq. (15). Aside from a typo in the first line of Eq. (28) in our previous work [6], i.e., $E_{n\mathbf{k}}$ is supposed to be $E_{n\mathbf{k}}^3$ in the denominator, Eq. (16) proves to be a more convenient alternative expression for C_{ij}^{inter} when considering the dilute limit below. Similar to c_{ij}^{inter} , it is pleasing to note that C_{ij}^{inter} also does not have any contribution from the band touchings, i.e., the first term of Eq. (16) cancels those touching contributions from the second term whenever $\xi_{n\mathbf{k}} = \xi_{m\mathbf{k}}$ for any $n \neq m$.

In accordance with the literature [27], we define the zero-temperature coherence length as

$$(\xi_0^2)_{ij} = \frac{C_{ij}}{A}, \quad (17)$$

assuming $C_{ij} > 0$. Here, $C_{ij} < 0$ signals that the minimum of $\mathcal{M}_{11}^q + \mathcal{M}_{12}^q$ occurs at a finite \mathbf{q} [29], depending on the symmetries of the underlying lattice geometry. In such cases, the low- \mathbf{q} expansion must be performed around the new minimum instead of $\mathbf{q} = \mathbf{0}$. Similar to ξ_{GL} , Eq. (17) suggests that ξ_0 is also composed of a conventional contribution $(\xi_0^2)_{ij}^{\text{intra}} = C_{ij}^{\text{intra}}/A$ and a geometric one $(\xi_0^2)_{ij}^{\text{inter}} = C_{ij}^{\text{inter}}/A$. Here, the calculation of ξ_0 requires self-consistent solutions of μ and Δ_0 as inputs. In the usual zero-temperature BCS-BEC crossover formalism [6, 28], these parameters are determined by the saddle-point condition $1 = \frac{U}{N} \sum_{n\mathbf{k}} 1/(2E_{n\mathbf{k}})$ and the mean-field number equation $F = F_0 = 1 - \frac{1}{N} \sum_{n\mathbf{k}} \xi_{n\mathbf{k}}/E_{n\mathbf{k}}$. In sharp contrast to the finite-temperature recipe of Sec. III, which requires

Gaussian corrections to the number equation, this simple mean-field recipe is known to be sufficient in producing a qualitatively correct physical description of the system for all $U \neq 0$. In fact, in the case of a three-dimensional continuum model with a quadratic dispersion, ξ_0 and ξ_{GL} are known to give very similar results up to a constant of order unity for all $U \neq 0$ [27]. However, this is not in general the case for a single-band lattice model with cosine dispersion away from the dilute limit, where C_{ij} can change sign and become negative for some intermediate U values [29]. See Appendix A for such a breakdown in the pyrochlore lattice.

Before delving into the heavy numerical calculations, here we highlight an important analytical insight for the pyrochlore lattice. In the dilute flat-band limit when $F \ll 1$, one can show that $\mu + 2t < 0$ and $|\mu + 2t| \gg \Delta_0$ for all $U \neq 0$. For instance, this can be verified by taking the $F \rightarrow 0$ limit of $\Delta_0 = \frac{U}{2}\sqrt{F(1-F)}$ and $\mu = -2t - \frac{U}{4}(1-2F)$ in the $U/t \ll 1$ limit, and of $\Delta_0 = \frac{U}{2}\sqrt{F(2-F)}$ and $\mu = -\frac{U}{2}(1-F)$ in the $U/t \gg 1$ limit. Thus, since $\xi_{\mathbf{n}\mathbf{k}} \gg \Delta_0$ for any $U \neq 0$, we may set $E_{\mathbf{n}\mathbf{k}} \rightarrow \xi_{\mathbf{n}\mathbf{k}}$, leading to $A = \frac{1}{N} \sum_{\mathbf{n}\mathbf{k}} \Delta_0^2 / (2\xi_{\mathbf{n}\mathbf{k}}^3)$ for the static coefficient, $C_{ij}^{\text{intra}} = \frac{1}{N} \sum_{\mathbf{n}\mathbf{k}} \xi_{\mathbf{n}\mathbf{k}}^i \xi_{\mathbf{n}\mathbf{k}}^j / (8\xi_{\mathbf{n}\mathbf{k}}^3)$ for the conventional kinetic coefficient, and $C_{ij}^{\text{inter}} = \frac{1}{2N} \sum_{\mathbf{n}\mathbf{k}} g_{ij}^{\mathbf{n}\mathbf{k}} / (2\xi_{\mathbf{n}\mathbf{k}}) - \frac{1}{2N} \sum_{\mathbf{n}, \mathbf{m} \neq \mathbf{n}, \mathbf{k}} g_{ij}^{\mathbf{n}\mathbf{m}\mathbf{k}} / (\xi_{\mathbf{n}\mathbf{k}} + \xi_{\mathbf{m}\mathbf{k}})$ for the geometric kinetic coefficient. Similarly, since $\xi_{\mathbf{n}\mathbf{k}} \gg T_c$ for any $U \neq 0$ in the $F \ll 1$ limit, we may set $\mathcal{X}_{\mathbf{n}\mathbf{k}} \rightarrow 1$ and $\mathcal{Y}_{\mathbf{n}\mathbf{k}} \rightarrow 0$ in Eqs. (4), (6) and (7), leading to $a_0 = -\frac{T_c}{2N} \frac{\partial \mu}{\partial T} \Big|_{T_c} \sum_{\mathbf{n}\mathbf{k}} 1/\xi_{\mathbf{n}\mathbf{k}}^2$ for the static coefficient, and $c_{ij}^{\text{intra}} = 2C_{ij}^{\text{intra}}$ and $c_{ij}^{\text{inter}} = 2C_{ij}^{\text{inter}}$ for the kinetic coefficients. Note that a prefactor of 2 difference arises from the distinct definitions used in the low- \mathbf{q} expansions of $\Gamma_0^{-1}(\mathbf{q})$ and $\mathcal{M}_{11}^{\mathbf{q}} + \mathcal{M}_{12}^{\mathbf{q}}$. Thus, in the dilute limit, we find that $(\xi_0^2)_{ij} / (\xi_{\text{GL}}^2)_{ij} = a_0/A$ for all $U \neq 0$, assuming these length scales are nonzero.

V. NUMERICAL RESULTS

In Fig. 1, we present self-consistent solutions of Eqs. (11) and (12) as functions of U/t for various particle fillings. Here, we recall that the scattering-state contribution F_{sc} to the number equation is not included in our simplified recipe, i.e., $F = F_0 + F_{bs}$. Therefore, our numerical results are expected to be accurate in parameter regimes where either the saddle-point or the bound-state contribution dominate. This occurs when either $F_0/F \rightarrow 1$ leading to the BCS limit, or $F_{bs}/F \rightarrow 1$ leading to the BEC limit. Figure 1(a) suggests that our approximations are well-justified for all $U/t \neq 0$ for a dilute flat-band superconductor with $F \ll 1$, and for $U/t \gg 1$ in general for higher fillings. In this paper, we are not concerned with those fillings where μ overlaps with a dispersive band in the non-interacting limit. In such cases, similar to the usual BCS-BEC crossover problem [22, 26], our recipe can also be justified in both the low- U/t and high- U/t regimes, but not in the intermediate crossover

region.

The corresponding T_c data are presented in Fig. 1(b). We observe that after T_c rises almost linearly for small $U \lesssim t$, it reaches a peak around $U \sim 5t$ and then decays as t^2/U for $U \gg t$. These results are consistent with recent works on the Berezinskii-Kosterlitz-Thouless (BKT) transition temperature T_{BKT} of two-dimensional flat-band models, which are based on the universal-jump relation involving the superfluid-weight tensor [1, 3]. In comparison, we also present the mean-field temperature scale T_{mf} , which is calculated by setting $F_{bs} = 0$ in Eq. (12). Unlike T_c , which marks the onset of phase coherence among Cooper pairs, T_{mf} is associated with the formation of pairs and increases without bound as a function of U/t [22, 26]. In other words, the dissociation temperature of pairs increases with their binding energy. Thus, in a flat-band superconductor, Fig. 1(b) shows that the formation and condensation of Cooper pairs occur at very different temperature scales for any $U \neq 0$, and the BCS theory must be used with caution. While T_c and T_{BKT} are governed directly by the quantum geometry of the Bloch states through F_{bs} and superfluid weight, respectively, in three and two dimensions, T_{mf} is not.

After computing the self-consistent solutions for μ and T_c as functions of U , the next step involves finding an efficient method to approximate $\frac{\partial \mu}{\partial T} \Big|_{T_c}$, which is necessary for defining ξ_{GL} as it appears in Eq. (4). From the usual BCS-BEC crossover problem, we know that $\frac{\partial \mu}{\partial T} \rightarrow 0$ in the BCS limit, whereas it controls the dominant contribution to a_0 in the BEC limit [22]. Thus, to properly capture the BEC limit, we recall the following insights from the Bogoliubov theory of a weakly-interacting atomic Bose gas [30]: (i) the density of condensed bosons is given by $n_0(T) = n_B [1 - (T/T_c)^{\frac{3}{2}}]$ for $T < T_c$, and (ii) the chemical potential of superfluid bosons is given by $\mu_B(T) = U_{\text{BB}} n_0(T) > 0$. Here, n_B is the total density of condensed and noncondensed bosons, and U_{BB} is their onsite repulsion. By making an analogy with $\mu_p = 2\mu - E_b$ of the Cooper pairs that is derived in Sec. III, we approximate $\frac{\partial \mu}{\partial T} \Big|_{T_c} = \frac{1}{2} \frac{\partial \mu_p}{\partial T} \Big|_{T_c} = -3U_{pp} F_p / (4T_c)$, where $U_{pp} = 2U$ is discussed below and $F_p = F_{bs}/2$.

In Fig. 2, we present self-consistent solutions for $1/M_p$ and ξ_{GL} as functions of U/t for various particle fillings. Here, $(M_p^{-1})_{ij} = \delta_{ij}/M_p$ and $(\xi_{\text{GL}}^2)_{ij} = \xi_{\text{GL}}^2 \delta_{ij}$ for the pyrochlore lattice as a consequence of uniform pairing. Similar to the overall shape of the T_c data, we observe that $1/M_p$ rises almost linearly for small $U \lesssim t$, it reaches a peak around $U \sim 5t$ and then decays as t^2/U for $U \gg t$. This similarity is reminiscent of the BEC transition temperature $T_c \propto n_B^{2/3}/M_B$ of an ideal Bose gas [30]. Furthermore, Fig. 2(a) shows that $1/M_p$ depends weakly on F for all U , especially in the BEC limit when $F_{bs}/F \rightarrow 1$. This is because, by construction, our TDGL theory reproduces the exact effective mass M_b of the lowest-lying two-body bound states (i) in the $F \ll 1$ limit for any $U/t \neq 0$, and (ii) in the $U/t \rightarrow \infty$ limit for any filling [5]. On the other hand, Fig. 2(b) shows that ξ_{GL} de-

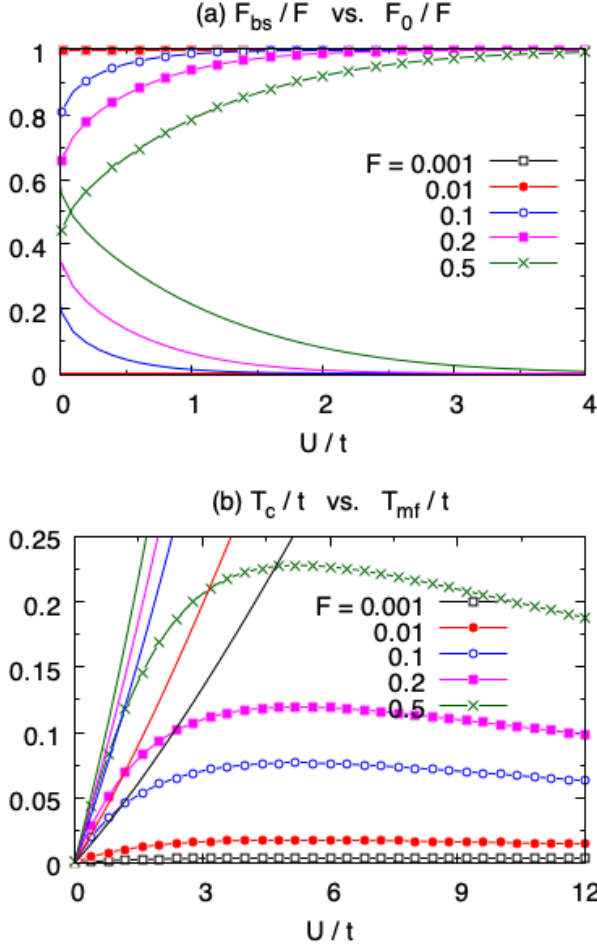


FIG. 1. Fractions of bound-state contribution (line plots with data points) and saddle-point contribution (line plots) are shown in (a) as functions of interaction strength for various fillings. The data for fillings $F = 0.01$ and $F = 0.001$ are indistinguishable on the presented scale. Corresponding critical temperatures (line plots with data points) are shown in (b), and compared with the mean-field temperature scales (line plots).

cays to zero monotonously without bound as a function of U/t . There, we also present self-consistent solution for the zero-temperature coherence length ξ_0 as defined by Eq. (17), where $(\xi_0^2)_{ij} = \xi_0^2 \delta_{ij}$ for the pyrochlore lattice due again to uniform pairing. In the $F \ll 1$ limit, it is delightful to see that ξ_{GL} and ξ_0 length scales are approximately equal to each other, differing only by a prefactor of order unity. Thus, despite all of the approximations involved in the calculation of ξ_{GL} , this benchmark demonstrates that our finite-temperature recipe produces accurate results for the dilute flat-band limit in the pyrochlore lattice. See Appendix A for greater details about ξ_0 in the pyrochlore lattice.

To gain further physical insight into these numerical observations, we examine two specific limits. For instance, in the $U/t \rightarrow 0$ limit when $\mu + 2t < 0$ and

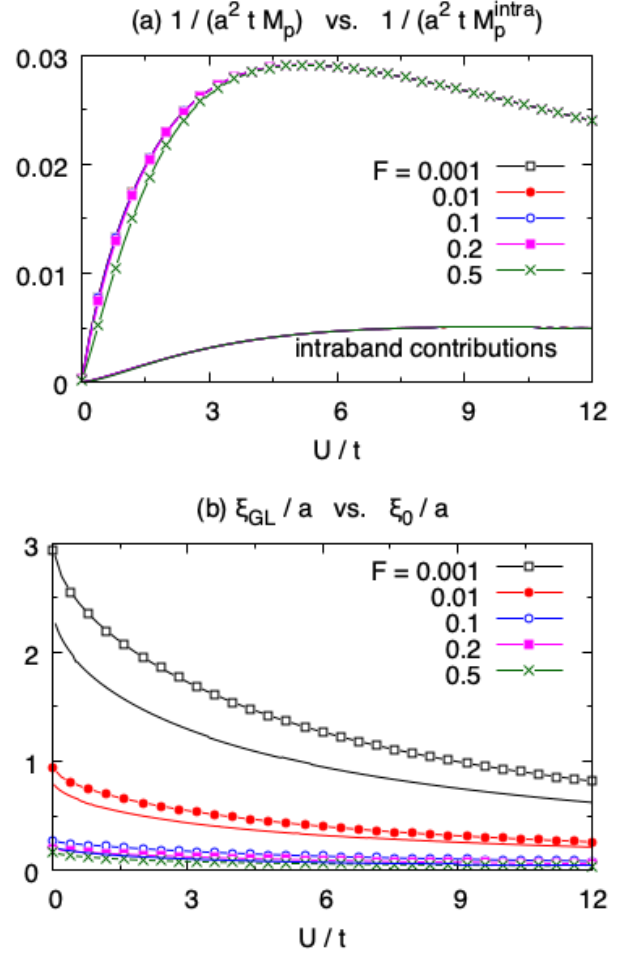


FIG. 2. The effective mass of the Cooper pairs (line plots with data points) and its conventional intraband contribution (line plots) are shown in (a) as functions of interaction strength for various fillings. Except for the $F = 0.5$ data, these are indistinguishable from the effective mass of the lowest-lying two-body bound states [6] on the presented scale. Corresponding Ginzburg-Landau coherence lengths (line plots with data points) are shown in (b), and compared with the zero-temperature coherence lengths (line plots). The latter is not shown for $F = 0.2$ and $F = 0.5$ data where it is not valid.

$|\mu + 2t| \gg T_c$, i.e., when $F \ll 1$, we find $\mu = -2t - U/4$, suggesting that $\xi_{n\mathbf{k}} \gg T_c$. Thus, by keeping only the flat-band contributions in the \mathbf{k} sums, we find $a_0 = 3F_{bs}/(8|\mu + 2t|)$ for the static coefficient, where $F_{bs} \rightarrow F$ in this limit as shown in Fig. 1(a), $b_0 = 1/(8|\mu + 2t|^3)$ for the quartic coefficient, $c_{ij}^{intra} = 0$ and $c_{ij}^{inter} = \frac{1}{2|\mu+2t|N} \sum'_{f,m \notin f, \mathbf{k}} g_{ij}^{f m \mathbf{k}}$ for the kinetic coefficients, where $f = \{3, 4\}$ refers to the flat bands and $m = \{1, 2\}$ refers to the dispersive bands (the prime sum excludes the band touchings), and $d = 1/(8|\mu + 2t|^2)$ for the dynamic coefficient. They lead to $(M_p^{-1})_{ij} = \frac{|\mu+2t|}{N} \sum'_{f,m \notin f, \mathbf{k}} g_{ij}^{f m \mathbf{k}}$ for the effective-mass of the Cooper pairs, $U_{pp} = 8|\mu + 2t|$ for the onsite repulsion between the pairs, and $(\xi_{GL}^2)_{ij} =$

$\frac{1}{6F_{bs}N} \sum_{f,m \neq f, \mathbf{k}}' g_{ij}^{f m \mathbf{k}}$ for the GL coherence length among the pairs. It is pleasing to note that $U_{pp} \rightarrow 2U$ is consistent with the low-energy collective-mode analysis at $T = 0$ [6]. A more suggestive way to express the latter result is $\xi_{GL} = \sqrt{2/(3U_{pp}M_pF_p)}$, which is approximately equal to the Bogoliubov expression $\xi_B = \sqrt{1/(2U_{BB}M_B F_B)}$ of a superfluid Bose gas [30], differing only by a prefactor of order unity. Similarly, in the same limit, we find $A = 4F(1-F)/U \rightarrow 4F/U$ for the static coefficient, and recall $C_{ij} = c_{ij}/2$ as derived in Sec. IV. They lead to $\xi_0 = 1/\sqrt{4U_{pp}M_pF_p}$, which again differs only by a prefactor of order unity. This result shows that $\xi_0 < \xi_{GL}$, which is consistent with Fig. 2(b).

In the other limit when $U/t \rightarrow \infty$, by noting that $\mu \rightarrow -U/2$ and $\xi_{n\mathbf{k}} \gg T_c$, we find $a_0 = 3F_{bs}/(4|\mu|)$ for the static coefficient, where $F_{bs} \rightarrow F$ in this limit as shown in Fig. 1(a), $b_0 = 1/(4|\mu|^3)$ for the quartic coefficient, $c_{ij}^{\text{intra}} = \frac{1}{4|\mu^3|N} \sum_{n\mathbf{k}} Q_{ij}^{n\mathbf{k}}$ for the conventional kinetic coefficient, $c_{ij}^{\text{inter}} = \frac{1}{4|\mu^3|N} \sum_{n,m \neq n, \mathbf{k}} Q_{ij}^{n\mathbf{k}}$ for the geometric kinetic coefficient, and $d = 1/(4\mu^2)$ for the dynamic coefficient. Here, we define $Q_{ij}^{n\mathbf{k}} = \text{Re}[\langle n_{\mathbf{k}} | \dot{\mathbf{h}}_{\mathbf{k}}^i | m_{\mathbf{k}} \rangle \langle m_{\mathbf{k}} | \dot{\mathbf{h}}_{\mathbf{k}}^j | n_{\mathbf{k}} \rangle]$, where $\dot{\mathbf{h}}_{\mathbf{k}}^i = \partial \mathbf{h}_{\mathbf{k}} / \partial k_i$ is the derivative of the Bloch Hamiltonian. This leads to $Q_{ij}^{n\mathbf{k}} = \varepsilon_{n\mathbf{k}}^i \varepsilon_{n\mathbf{k}}^j$ for the intraband processes, and $Q_{ij}^{n \neq m \mathbf{k}} = \frac{1}{2}(\varepsilon_{n\mathbf{k}} - \varepsilon_{m\mathbf{k}})^2 g_{ij}^{n\mathbf{k}}$ for the interband processes. In deriving c_{ij}^{inter} , we also observed that $\sum_{n,m \neq n, \mathbf{k}} (\varepsilon_{n\mathbf{k}} - \varepsilon_{m\mathbf{k}}) g_{ij}^{n\mathbf{k}} = 0$ and $\sum_{n,m \neq n, \mathbf{k}} (\varepsilon_{n\mathbf{k}}^2 - \varepsilon_{m\mathbf{k}}^2) g_{ij}^{n\mathbf{k}} = 0$ since $g_{ij}^{n\mathbf{k}} = g_{ji}^{m\mathbf{k}}$ and $g_{ij}^{n\mathbf{k}} = g_{ji}^{n\mathbf{k}}$ by definition. Thus, the total kinetic coefficient can be calculated via the identity $\sum_{n\mathbf{k}} \langle n_{\mathbf{k}} | \dot{\mathbf{h}}_{\mathbf{k}}^i | m_{\mathbf{k}} \rangle \langle m_{\mathbf{k}} | \dot{\mathbf{h}}_{\mathbf{k}}^j | n_{\mathbf{k}} \rangle = \sum_{\mathbf{k}} \text{Tr}[\dot{\mathbf{h}}_{\mathbf{k}}^i \dot{\mathbf{h}}_{\mathbf{k}}^j] = Nca^2 t^2 \delta_{ij}$, suggesting that $c_{ij} = a^2 t^2 \delta_{ij} / (16|\mu|^3)$. Together with the rest of the coefficients, they lead to $(M_p^{-1})_{ij} = a^2 t^2 \delta_{ij} / (4|\mu|)$ for the effective-mass of the Cooper pairs, $U_{pp} = 4|\mu|$ for the onsite repulsion between the pairs, and $(\xi_{GL}^2)_{ij} = a^2 t^2 \delta_{ij} / (12U|\mu|F)$ for the GL coherence length among the pairs. It is pleasing to note that $M_p = 2U/(a^2 t^2)$ and $U_{pp} \rightarrow 2U$ are again consistent with the low-energy collective-mode analysis at $T = 0$ [6]. The latter result can be written in a more suggestive way $\xi_{GL} = 1/\sqrt{3U_{pp}M_pF_p}$. Similarly, in the same limit, we find $A = F(2-F)/U \rightarrow 2F/U$ for the static coefficient, and recall that $C_{ij} = c_{ij}/2$, leading to $\xi_0 = 1/\sqrt{4U_{pp}M_pF_p}$. Thus, we again conclude that ξ_{GL} and ξ_0 differ from each other and from ξ_B by factors of order unity, reflecting the dilute-limit behavior. Moreover, $\xi_0 < \xi_{GL}$, which is consistent with Fig. 2(b).

VI. CONCLUSION

In summary, we developed a self-consistent formulation of the GL coherence length ξ_{GL} in a dilute flat-band superconductor using the multiband pyrochlore-Hubbard

model. Our results are highly consistent with the zero-temperature coherence length ξ_0 , demonstrating that ξ_{GL} decreases to zero monotonously as U/t increases. Furthermore, we established that the effective mass of Cooper pairs aligns closely with that of the lowest-lying two-body bound states in the dilute regime. As an outlook, we plan to improve the quantitative accuracy of these findings by implementing a more accurate number equation near T_c . For instance, similar to the crucial role played by the bound-state contribution F_{bs} in the dilute flat-band limit, we expect that the scattering-state contribution F_{sc} will become equally important at and around the half-filled flat-band limit. Although we do not expect any qualitative change, inclusion of F_{sc} is inevitable there, especially in the low- U/t regime. Furthermore, there is room for improvement in the calculation of F_{bs} , e.g., by extracting $\omega_{b\mathbf{q}}$ more accurately without relying on the two-body results, or by incorporating contribution from other poles.

ACKNOWLEDGMENTS

The author acknowledges funding from US Air Force Office of Scientific Research (AFOSR) Grant No. FA8655-24-1-7391.

Appendix A: Breakdown of $(\xi_0^2)_{ij}$

By definition, the zero-temperature coherence length $(\xi_0^2)_{ij}$ is not well-defined in the parameter regime where C_{ij} is negative. In Fig. 3(a), we present $\xi_0^2 < 0$ values in the unphysical region as a function of U/t and F , indicating that ξ_0 can be meaningfully defined for the dilute flat-band ($F \ll 1$) limit of our interest in the pyrochlore lattice. Similar to the well-studied continuum model with a quadratic dispersion [27], this is known to be the case for a dilute single-band lattice model with cosine dispersion [29], where ξ_0 and ξ_{GL} are known to give very similar results up to a constant of order unity for all $U \neq 0$. When $C_{ij} < 0$, it signals that the minimum of $\mathcal{M}_{11}^{\mathbf{q}} + \mathcal{M}_{12}^{\mathbf{q}}$ occurs at a finite \mathbf{q} . If desired, one can perform the low- \mathbf{q} expansion around the new minimum instead of $\mathbf{q} = \mathbf{0}$, and define $(\xi_0^2)_{ij}$ accordingly.

On the other hand, in Fig. 3(b), we present ξ_0 in the physical region as a function of U/t and F , showing that ξ_0/a scales with t/Δ_0 in most of the parameter space, except for the flat-band superconductivity in the low- U/t regime. There, ξ_0 is governed solely by the quantum geometry of the Bloch states. We note that a similar scaling has recently been reported in the arxiv for a distinct but a related correlation length in the context of the sawtooth lattice [21]. Thus, similar to the dilute case, ξ_0 decreases without bound as U/t increases for any F within the physical region.

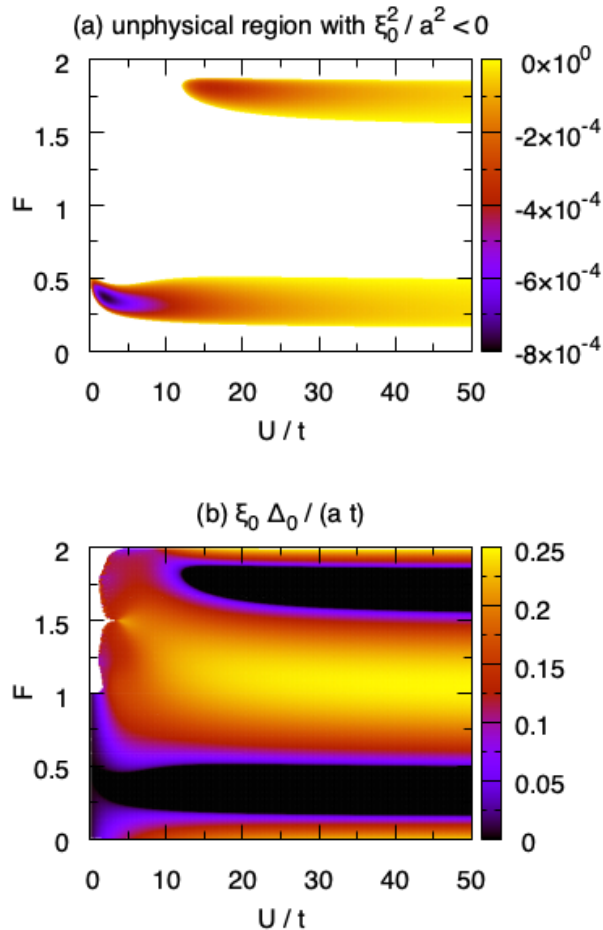


FIG. 3. The colored map of zero-temperature coherence length is shown in (a) for the unphysical region where $\xi_0^2 < 0$. In (b), ξ_0/a is shown to scale as t/Δ_0 in most of the physical region, except for the flat-band superconductivity in the low- U/t regime. Since our numerics becomes unreliable in the $\Delta_0/t \rightarrow 0$ limit, we present only the data with $\Delta_0/t > 0.001$, revealing the underlying single-particle density of states at the periphery of the white region [6], i.e., for the BCS limit when $1 < F < 2$.

-
- [1] P. Törmä, S. Peotta, and B. A. Bernevig, Superconductivity, superfluidity and quantum geometry in twisted multilayer systems, *Nature Reviews Physics* **4**, 528 (2022).
- [2] P. Törmä, Essay: Where can quantum geometry lead us?, *Phys. Rev. Lett.* **131**, 240001 (2023).
- [3] K.-E. Huhtinen, J. Herzog-Arbeitman, A. Chew, B. A. Bernevig, and P. Törmä, Revisiting flat band superconductivity: Dependence on minimal quantum metric and band touchings, *Phys. Rev. B* **106**, 014518 (2022).
- [4] J. Herzog-Arbeitman, A. Chew, K.-E. Huhtinen, P. Törmä, and B. A. Bernevig, Many-body superconductivity in topological flat bands (2022), [arXiv:2209.00007](https://arxiv.org/abs/2209.00007).
- [5] M. Iskin, Extracting quantum-geometric effects from Ginzburg-Landau theory in a multiband Hubbard model, *Phys. Rev. B* **107**, 224505 (2023).
- [6] M. Iskin, Cooper pairing, flat-band superconductivity, and quantum geometry in the pyrochlore-Hubbard model, *Phys. Rev. B* **109**, 174508 (2024).
- [7] A. Daido, T. Kitamura, and Y. Yanase, Quantum geometry encoded to pair potentials, (2023), [arXiv:2310.15558](https://arxiv.org/abs/2310.15558).
- [8] S. A. Chen and K. T. Law, Ginzburg-Landau theory of flat-band superconductors with quantum metric, *Phys. Rev. Lett.* **132**, 026002 (2024).
- [9] M. Thumin and G. Bouzerar, Constraint relations for superfluid weight and pairings in a chiral flat band superconductor, *Europhysics Letters* **144**, 56001 (2023).
- [10] N. Verma, D. Guerzi, and R. Queiroz, Geometric stiffness

- in interlayer exciton condensates, *Phys. Rev. Lett.* **132**, 236001 (2024).
- [11] G. Jiang and Y. Barlas, Geometric superfluid weight of composite bands in multiorbital superconductors, *Phys. Rev. B* **109**, 214518 (2024).
- [12] M. Iskin, Quantum-metric contribution to the pair mass in spin-orbit-coupled Fermi superfluids, *Phys. Rev. A* **97**, 033625 (2018).
- [13] M. Iskin, Berezinskii-Kosterlitz-Thouless transition in the time-reversal-symmetric Hofstadter-Hubbard model, *Phys. Rev. A* **97**, 013618 (2018).
- [14] P. Törmä, L. Liang, and S. Peotta, Quantum metric and effective mass of a two-body bound state in a flat band, *Phys. Rev. B* **98**, 220511 (2018).
- [15] M. Iskin, Effective-mass tensor of the two-body bound states and the quantum-metric tensor of the underlying Bloch states in multiband lattices, *Phys. Rev. A* **105**, 023312 (2022).
- [16] L. Balents, C. R. Dean, D. K. Efetov, and A. F. Young, Superconductivity and strong correlations in Moiré flat bands, *Nat. Phys.* **16**, 725 (2020).
- [17] H. Tian, X. Gao, Y. Zhang, S. Che, T. Xu, P. Cheung, K. Watanabe, T. Taniguchi, M. Randeria, F. Zhang, *et al.*, Evidence for Dirac flat band superconductivity enabled by quantum geometry, *Nature* **614**, 440 (2023).
- [18] J. P. Wakefield, M. Kang, P. M. Neves, D. Oh, S. Fang, R. McTigue, S. Frank Zhao, T. N. Lamichhane, A. Chen, S. Lee, *et al.*, Three-dimensional flat bands in pyrochlore metal CaNi₂, *Nature* **623**, 301 (2023).
- [19] J. Huang, C. Setty, L. Deng, J.-Y. You, H. Liu, S. Shao, J. S. Oh, Y. Guo, Y. Zhang, Z. Yue, *et al.*, Observation of flat bands and Dirac cones in a pyrochlore lattice superconductor, (2023), [arXiv:2304.09066](https://arxiv.org/abs/2304.09066).
- [20] J.-X. Hu, S. A. Chen, and K. Law, Anomalous coherence length in superconductors with quantum metric, (2023), [arXiv:2308.05686](https://arxiv.org/abs/2308.05686).
- [21] M. Thumin and G. Bouzerar, Correlation functions and characteristic lengthscales in flat band superconductors, arXiv preprint [arXiv:2405.06215](https://arxiv.org/abs/2405.06215) (2024).
- [22] C. A. R. Sá de Melo, M. Randeria, and J. R. Engelbrecht, Crossover from BCS to Bose superconductivity: Transition temperature and time-dependent Ginzburg-Landau theory, *Phys. Rev. Lett.* **71**, 3202 (1993).
- [23] J. P. Provost and G. Vallee, Riemannian structure on manifolds of quantum states, *Commun. Math. Phys.* **76**, 289 (1980).
- [24] M. V. Berry, Quantal phase factors accompanying adiabatic changes, *Proceedings of the Royal Society of London. A. Mathematical and Physical Sciences* **392**, 45 (1984).
- [25] R. Resta, The insulating state of matter: a geometrical theory, *The European Physical Journal B* **79**, 121 (2011).
- [26] P. Nozieres and S. Schmitt-Rink, Bose condensation in an attractive fermion gas: From weak to strong coupling superconductivity, *J. Low Temp. Phys.* **59**, 195 (1985).
- [27] F. Pistolesi and G. C. Strinati, Evolution from BCS superconductivity to Bose condensation: Calculation of the zero-temperature phase coherence length, *Phys. Rev. B* **53**, 15168 (1996).
- [28] J. R. Engelbrecht, M. Randeria, and C. A. R. Sá de Melo, BCS to Bose crossover: Broken-symmetry state, *Phys. Rev. B* **55**, 15153 (1997).
- [29] L. Benfatto, A. Toschi, S. Caprara, and C. Castellani, Coherence length in superconductors from weak to strong coupling, *Phys. Rev. B* **66**, 054515 (2002).
- [30] A. L. Fetter and J. D. Walecka, *Quantum Theory of Many-Particle Systems* (McGraw-Hill, Boston, 1971).